STRUCTURAL SCIENCE
CRYSTAL ENGINEERING
MATERIALS

ISSN: 2052-5206
journals.iucr.org/b

# Predicting co-crystal structures of *N*-halide phthalimides with 3,5-dimethylpyridine

**Zahrasadat Momenzadeh Abardeh, Faezeh Bahrami and Artem R. Oganov**

*Acta Cryst.* (2024). B**80**, 620–627

Acta Cryst B STRUCTURAL SCIENCE CRYSTAL ENGINEERING MATERIALS

ISSN 2052-5206

# Predicting co-crystal structures of *N*-halide phthalimides with 3,5-dimethylpyridine

**Zahrasadat Momenzadeh Abardeh,[a] Faezeh Bahrami[b] and Artem R. Oganov[a]***

[a]Skolkovo Institute of Science and Technology, Skolkovo Innovation Center, Moscow, 121205, Russian Federation, and [b]Department of Chemistry, Faculty of Science, Ferdowsi University of Mashhad, Mashhad, Iran. *Correspondence e-mail: a.oganov@skoltech.ru

Received 15 May 2024
Accepted 12 October 2024

Edited by P. Macchi, Politecnico di Milano, Italy

This article is part of a collection of articles covering the seventh crystal structure prediction blind test.

**Keywords:** co-crystal structure prediction; crystal engineering; halogen bonding; *N*-halide phthalimides; Cambridge Structural Database.

**Supporting information:** this article has supporting information at journals.iucr.org/b

Crystal structure prediction (CSP) calculations were carried out to examine potential formation of co-crystals between *N*-halide phthalimides (Cl, Br or I) and 3,5-dimethylpyridine (**35DMP**). The co-crystal structure of *N*-bromophthalimide (**nbp**) with **35DMP** (**nbp-35DMP**) is known, and the generated co-crystal structure of rank 1 is identical to experimental structure (VELXES). For the unknown crystal structure of *N*-iodophthalimide (**nip**), structure of rank 1 is suggested as a likely co-crystal structure. On the other hand, our calculations suggest the improbability of co-crystal formation between **ncp** and **35DMP**. The CSP findings indicate that strong N—X···N interactions consistent with similar experimental structures in the Cambridge Structural Database play a major role in crystal structures of the studied compounds.

## 1. Introduction

Crystal engineering seeks to understand how molecules interact within crystals, aiming to design new solid materials with specific physical and chemical properties (Oganov, 2011; Braga *et al.*, 2018; Greenwell & Beran, 2020; Mukherjee *et al.*, 2020; Bowskill *et al.*, 2021). Experimental methods such as single-crystal X-ray diffraction (SCXRD) and structure determination from powder diffraction (SDPD) are usually employed to determine crystal structures (Aakeröy, 1997; Desiraju, 2007; An *et al.*, 2020; Bolla *et al.*, 2022; Kabova *et al.*, 2022). However, these methods face some limitations, such as the challenge of preparing a single crystal (Bond & Jones, 2002; Harper & Grant, 2006; Baias *et al.*, 2013; Yao *et al.*, 2020; Chan *et al.*, 2021) or reliable indexing of powder diffraction patterns containing too few or too broad reflections, or if the powder is not phase-pure (Brüning & Schmidt, 2015; Habermehl *et al.*, 2022). In this context, crystal structure prediction (CSP) plays a crucial role. CSP has evolved into a valuable tool, particularly due to advancements in computing power and methods (Day *et al.*, 2006; Wang *et al.*, 2010; King *et al.*, 2011).

Considerable attention has been dedicated to the design and synthesis of co-crystals since they provide a way to modify the physicochemical properties of molecular compounds. In the pharmaceutical industry, co-crystals emerge as an innovative category of substances with the potential to improve various properties, such as solubility, dissolution rate, chemical stability, and physical stability (Sun *et al.*, 2020; Thayyil *et al.*, 2020; Bennion & Matzger, 2021; Wong *et al.*, 2021). Motivated by our recent research on predicting *N*-halide phthalimide compounds (Momenzadeh Abardeh *et al.*, 2022), this article explores how these molecules interact in co-crystals with 3,5-dimethylpyridine (**35DMP**).

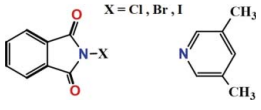

Momenzadeh Abardeh *et al.* (2022) demonstrated that in crystal structures composed of molecules similar to *N*-halide phthalimide, halogen bond N—X···O of type II plays a particularly important role among all possible N—X···O/X halogen bonds. Type II halogen bonding was used as a touchstone to select likeliest structures among the results of CSP of *N*-halide phthalimide compounds. The selected structures based on the halogen bonding were consistent with the experimental structures of *N*-chlorophthalimide (WEZVIG) (Ghassemzadeh *et al.*, 1994) and *N*-bromophthalimide (VELWIV and VELWIV01) (Eraković *et al.*, 2018; Momenzadeh Abardeh *et al.*, 2022), and two structures were suggested for the unknown crystal structure of *N*-iodophthalimide.

In crystal engineering, halogen bonding has gained significant attention in recent decades (Stilinović *et al.*, 2017; Teyssandier *et al.*, 2020; Kumar *et al.*, 2023). Halogen bonding involves an attractive interaction between an electron donor (nucleophile) and the $\sigma$-hole of a halogen atom (Fotović *et al.*, 2021; Guo *et al.*, 2022; Seidler *et al.*, 2022). It stands out among other interactions in its family due to the easily accessible $\sigma$-hole, resulting in strong and directed interactions (Politzer *et al.*, 2013; Mukherjee *et al.*, 2014; Varadwaj *et al.*, 2019).

Momenzadeh Abardeh *et al.* (2022) showed that halogen atoms prefer bonding with an oxygen atom rather than a halogen atom. These results sparked our curiosity about understanding how these compounds would interact when the potential for N—X···N halogen bonding was added. To explore this, we chose **35DMP** as a coformer, which has *N*-aromatic groups to form the *N*-halide phthalimide co-crystal. The Cambridge Structural Database (CSD) analysis of co-crystal structures similar to our compounds, containing *N*-aromatic atoms, demonstrates the replacement of the strong N—X···N interaction with the type II of N—X···O halogen bond (Castro *et al.*, 2007; Politzer *et al.*, 2007; Politzer *et al.*, 2010; Albright *et al.*, 2017; Tupikina *et al.*, 2020; Momenzadeh Abardeh *et al.*, 2022; Hein & Beer, 2022).

In this study, we explored the co-crystal structures of *N*-halide phthalimide with **35DMP** (Fig. 1). While a co-crystal structure of nbp with **35DMP** (VELXES) (Eraković *et al.*, 2018) has been previously reported, the crystal structures for *N*-chlorophthalimide (**ncp**) and *N*-iodophthalimide (**nip**) have not been reported yet. To explore the series of *N*-halide phthalimide co-crystal structures with **35DMP**, we conducted CSP searches.

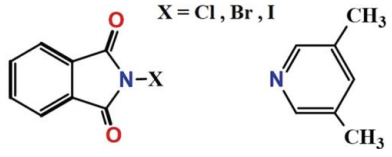


**Figure 1**
*N*-halide phthalimides (Cl, Br or I) and 3,5-dimethylpyridine (**35DMP**) In this study, we explored the co-crystal structures of *N*-halide phthalimide with **35DMP** (Fig. 1). While a co-crystal structure of nbp with **35DMP** (VELXES) (Eraković *et al.*, 2018) has been previously reported, the crystal structures for *N*-chlorophthalimide (**ncp**) and *N*-iodophthalimide (**nip**) have not been reported yet. To explore the series of *N*-halide phthalimide co-crystal structures with **35DMP**, we conducted CSP searches.

## 2. Methods

### 2.1. CSP calculations

The geometry of all molecules was optimized by density functional theory, using the *Gaussian09* (Frisch *et al.*, 2013) program and B3LYP/6-311g(p,d) basis set. The evolutionary algorithm implemented in the *USPEX 10.5* code (Oganov & Glass, 2006; Oganov *et al.*, 2011; Lyakhov *et al.*, 2013) was used to search for low-energy co-crystal structures. Co-crystal structures were generated in stoichiometry ratios of 1:1, 1:2, and 2:1. To generate structures, the common space groups ($P\overline{1}$, $P2$, $P2/c$, $P2/m$, $P2_1/c$, $Pbca$, $C2/c$, $Cc$, $Ccca$, $Pc$, $P2_12_12_1$, $Pbca$, $Pna2_1$, $Pnna$ and $Pca2_1$) were employed. The energy of structures at $T$ = 0 K and ambient pressure was used as measure of fit (see supporting information for more details). All generated structures were optimized using the GULP code (Gale & Rohl, 2003)/Dreiding force field (Mayo *et al.*, 1990) (atomic charges, Qeq) (Rappe & Goddard III, 1991). In the subsequent step, structures within 30 kJ mol$^{-1}$ of the global minimum were selected for each stoichiometric ratio. Structures with RMSD15 smaller than 0.2 Å (calculated using *Mercury* software; Macrae *et al.*, 2020) were considered identical. The resulting set of structures underwent re-optimization using the PBE-D3 dispersion-corrected functional (Perdew *et al.*, 1996; Grimme *et al.*, 2010) as implemented in the VASP code (Kresse & Furthmüller, 1996), and the projector augmented wave (PAW) method (Joubert & Kresse, 1999). The plane wave kinetic energy cutoff of 600 eV, Brillouin zone sampling with a k-point grid of $2\pi \times 0.06$ Å$^{-1}$ resolution and convergence criteria of $1 \times 10^{-5}$ eV per atom for total energies and $5 \times 10^{-3}$ eV Å$^{-1}$ for forces were employed. Additional details can be found in the supporting information.

### 2.2. CSD analysis

The CSD search aimed to find structural motifs in co-crystal structures formed by molecules similar to our target compounds. We looked at compounds consisting of two different molecules: one with the imide group (O═C—NX—C═O) and the other with an aromatic ring containing the N atom. They have the potential to form CH···O/X/N hydrogen bonds and N—X···X/O/N halogen bonds of types I and II. The fragment in Fig. 2 was used in the search, comprising two segments. As depicted in Fig. 2, on the left-hand side, 7A represents any halogen atom (T1, defined with one bonded atom). On the right-hand side, the N atom is defined with two bonded atoms (T2), with the bonds defined as aromatic, and A representing 'any atom'. In CSD analysis we considered only fully ordered structures with an *R* factor of $\leq$0.075 and no errors, polymerization of molecules or ions (CSD version 5.45, updated November 2023; Groom *et al.*, 2016); this yielded 37 structures. The list of refcodes for these 37 co-crystal structures identified in the CSD search is provided in the supporting information. These structures were thoroughly analyzed using the *Mercury* code, with a focus on intermolecular interactions.

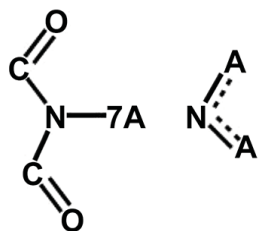


**Figure 2**
The fragment employed in the CSD search.

## 3. Results and discussion

### 3.1. CSD search

Analysis of experimental co-crystal structures in the CSD greatly helps to identify the type and geometry of the most significant interactions among all possible intermolecular interactions in the crystal structures of a set of similar molecules. This not only enhances our understanding of how different molecules connect to form co-crystal structures but also provides valuable guidance for identifying which of the structures obtained in CSP are more likely to form in an experiment (see below). Our CSD analysis indicates that the N—X···N synthon interaction plays a particularly important role in these co-crystal structures (Hein & Beer, 2022; Tupikina *et al.*, 2020; Albright *et al.*, 2017; Politzer *et al.*, 2010; Politzer *et al.*, 2007; Castro *et al.*, 2007). Furthermore, the C—H···O synthon interaction leads to connecting the N—X···N synthon interaction together in the co-crystal structures [Fig. 3(*a*)]. Analysis of the CSD reveals that the N—X···N halogen bond angle falls within the range 171–180°. Typically, C—H···*A* (*A* = X, O or N) hydrogen bonds exhibit geometries with a bond angle ranging from approximately 150° to 180°. It is noteworthy that for weaker interactions, the C—H···*A* angle tends to be smaller, often falling below 130° (Tupikina *et al.*, 2020; Castro *et al.*, 2007). Given that in all CSD co-crystal structures the N—X···N and C—H···O/N synthons play an important role [Fig. 3(*a*)], we expect to observe similar synthon interactions in the likely co-crystal structures of **nhp-35DMP** in the CSP.

Given that energy differences between different molecular crystal structures are usually very small, small errors in theoretical energies can change energy ranking of structures. On the other hand, while there can be many low-energy metastable structures, only a few of them (and not necessarily with the lowest energies) are experimentally synthesizable. Such kinetics factors are not easy to take into account directly (Thakur & Desiraju, 2008). However, the concept of synthons can be used to indicate structures that are likely both kinetically and thermodynamically (Dey *et al.*, 2005; Desiraju, 2007; Chakraborty & Desiraju, 2018; Momenzadeh Abardeh *et al.*, 2022). Synthons contain the most important structure-stabilizing interactions, hence thermodynamically stable structures are likely to have them. Besides, crystals grow from an

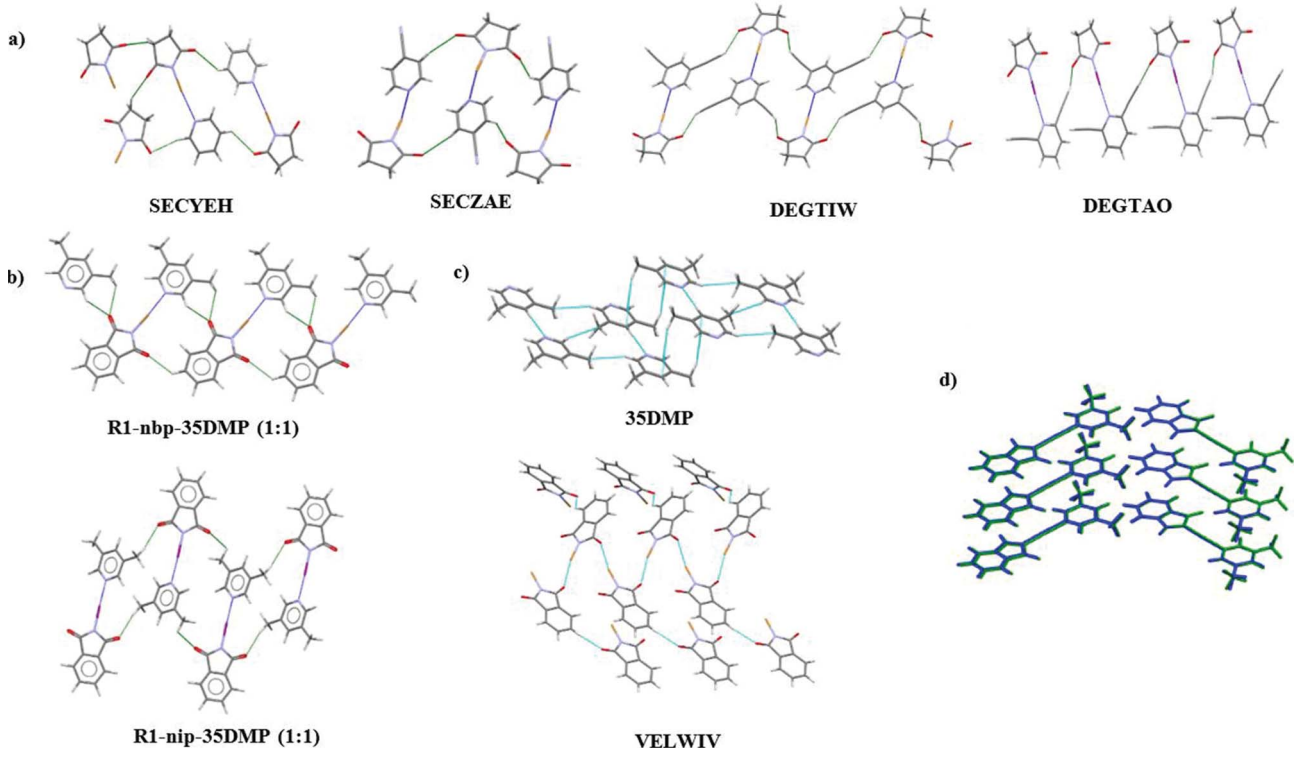


**Figure 3**
N—X···N halogen bond (blue) and C—H···O hydrogen bond (green) in: (*a*) the experimental co-crystal structures of SECYEH, SECZAE, DEGTIW, and DEGTAO; (*b*) the predicted co-crystal structures of rank 1 for **nbp-35DMP** and rank 1 **nip-35DMP**; (*c*) intermolecular interaction in crystal structures of pure **35DMP** (IDIGOR) and **nbp** (VELWIV); (*d*) overlap of structures rank 1 **nbp-35DMP** and VELXES (RMSD20 = 0.1 Å), where the experimental structure is colored green, and predicted rank 1 structure is colored dark blue.

environment where molecules are likely to form synthons, which serve as building blocks for the growing crystal; hence, kinetically favored polymorphs are also likely to contain synthons. Utilizing experimental synthons found from a set of co-crystal structures with similar molecules as criteria in CSP can be useful for selecting likely structures (Bond & Jones, 2002; Hofmann *et al.*, 2004; Thakur & Desiraju, 2008; Singh & Thakur, 2014; Momenzadeh Abardeh *et al.*, 2022). Here, we employ the found synthons in the CSD structures as a criterion for selecting likely co-crystal structures from among the generated structures (Momenzadeh Abardeh *et al.*, 2022).

Most of the experimental co-crystal structures are found at stoichiometric ratios of 1:1, with a few at a ratio of 1:2, in the common space groups of $P\overline{1}$, $P2$, $P2/c$, $P2/m$, $P2_1/c$, $Pbca$, $C2/c$, $Cc$, $Ccca$, $P2_12_12_1$, $Pbca$, $Pna2_1$, $Pnma$ and $Pc$. In the CSD search, we found only fragments with bromine and iodine atoms; no fragments with a chlorine atom were detected. This can be explained by the important role of the N—X···N halogen-bond interaction in the co-crystal of these structures, and the effect of the size and magnitudes of $\sigma$-holes on the halogen atom in this interaction (Lim & Beer, 2018).

Indeed, in the article by Lim & Beer, the $\sigma$-hole is discussed as follows: '*The strength of σ-hole interactions can be adjusted by varying the nature of the donor atom and the covalently bonded electron-withdrawing group. Larger donor atoms down a group are more polarizable and less electronegative, facilitating σ-hole formation with more Electron Sharing Points (ESPs). Among the halogens, the size and magnitudes of the σ-holes increase in the order of F < Cl < Br < I, and it is noteworthy that only the heavier halogens (Br and I) effectively serve as σ-hole donors in solution-phase anion recognition.*' (Clark *et al.*, 2007; Lim & Beer, 2018).

The molecular electrostatic potential (MEP) is a reliable method for identifying areas with electron deficits and surpluses in molecular systems, indicating electrophilic and nucleophilic sites. In this study, MEPs were calculated for **ncp**, **nbp**, and **nip** using the B3LYP/LANL2DZ method. Fig. 4 shows the MEP maps of *N*-halide phthalimide molecules, applied to 0.002 au electron density contours. Analysis of these maps reveals a $\sigma$-hole along the N—X covalent bond on the molecular surface of halogen atoms. Indeed, the size of the $\sigma$-hole increases with the size of the halogen atom, in the order Cl < Br < I.

In the crystal structures of pure *N*-halide phthalimides, N—X···O halogen bonding is crucial. In the crystal structure of pure 3,5-dimethylpyridine, C—H···N hydrogen bonding plays a key role, as shown in Fig. 3(*c*), which illustrates intermolecular interactions in the crystal structures of pure 35DMP (IDIGOR) and nbp (VELWIV). Based on the analysis of the CSD search, when these molecules connect to form a co-crystal, the halogen atom forms a robust N—X···N hydrogen bond instead of an N—X···O. This preference is guided by the strength of the $\sigma$-holes. Analysis of MEP maps of *N*-halide phthalimide molecules highlights that bromine and iodine, due to the size of the $\sigma$-hole, are well suited for N—X···N hydrogen bonding (Fig. 4). In contrast, the size of the $\sigma$-hole for the chlorine atom explains its inability to form

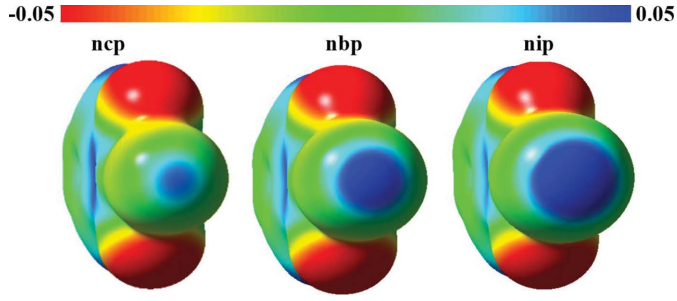


**Figure 4**
MEP maps of **ncp**, **nbp** and **nip** molecules mapped on the 0.002 au electron density contours at the B3LYP/LANL2DZ level of theory. The electrostatic potential varies from −0.05 (red) to +0.05 (blue) au.

N—X···N hydrogen bonding, resulting in the absence of a co-crystal containing chlorine in the CSD search. In other words, when crystals grow, whether they become pure crystals or co-crystals depends on the competition between different types of intermolecular interactions. If the C—H···O/X/N and N—X···O interactions are predominant, pure crystals form. However, if the N—X···N halogen bond between two different molecules is stronger, it promotes the formation of co-crystals. In the series of halides, the sizes and magnitudes of the $\sigma$-hole of the Cl atom, unlike those of the I and Br atoms, hinder the prevalence of the N—X···N halogen bond in competition with C—H···O/X/N and N—X···O interactions, leading to the formation of pure crystal structures.

Fig. 3 is useful for visualizing the concepts discussed. Fig. 3(*a*) illustrates how molecules in the CSD structures form co-crystals with a similar arrangement of the N—X···N halogen bond (colored in blue) and the C—H···O hydrogen bond (colored in green). Fig. 3(*b*) shows that the selected structures, rank 1 for **nbp-35DMP** and **nip-35DMP** exhibit an interaction pattern similar to that observed in the CSD structures shown in Fig. 3(*a*). As expected, the N—X···O halogen bond and the C—H···O and CH···N hydrogen bonds, shown in Fig. 3(*c*), represent the effective contacts in the crystal structures of pure compounds.

### 3.2. Thermodynamic convex hull

For each co-crystal stoichiometric ratio, a separate CSP was performed. To determine which stoichiometries are thermodynamically stable, we first calculate the normalized energies of formation $\Delta E(\mathrm{A}x\mathrm{B}y)$ of all possible co-crystals from pure A and B in their ground state.

$$\Delta E(\mathrm{A}x\mathrm{B}y) = \left[E(\mathrm{A}x\mathrm{B}y) - xE(\mathrm{A}) - yE(\mathrm{B})\right]/(x + y).$$

Here $E$(A) and $E$(B) represent the energies of pure crystals A and B, per molecule. A stable compound (in this case, a co-crystal) should have lower free energy than any isochemical phase assemblage [*i.e.* its point in Fig. 5 should be below any line drawn between any two points corresponding to other hypothetical compounds (co-crystals in this case)], which leads to the convex hull construction (Fig. 5). In the context of molecular crystals, all this is done under the constraint of a fixed conformation.

**Table 1**
List of the first ten generated co-crystal structures of **nbp-35DMP** and **nip-35DMP**, ranked by the height above the convex hull (dh).

Structures were relaxed using PBE-D3. Results for VELXES are reported for the unrelaxed experimental structure (relaxation yields the structure identical to our rank 1 structure). Z1 represents the number of **nbp** or **nip** molecules, and Z2 represents the number of **35DMP** molecules in the unit cell.

| Rank (dh) | Z1 | Z2 | Space group | Density (g cm$^{-3}$) | Composition | $\Delta E$ (kJ mol$^{-1}$) | Volume (Å$^3$/asymmetric unit) | dh (kJ mol$^{-1}$ per molecule) | N—X···N (°) |
|---|---|---|---|---|---|---|---|---|---|
| **nbp-35DMP** | | | | | | | | | |
| VELXES | 4 | 4 | $P2_1/c$ | 1.58 | 0.50 | −1.82 | 351.22 | 0.03 | 175.96 |
| 1 | 4 | 4 | $P2_1/c$ | 1.66 | 0.50 | −1.92 | 334.00 | 0.00 | 176.45 |
| 2 | 2 | 2 | $P\bar{1}$ | 1.65 | 0.50 | −1.50 | 335.15 | 0.11 | 167.15 |
| 3 | 4 | 2 | $P\bar{1}$ | 1.72 | 0.67 | −0.81 | 540.11 | 0.12 | 160.59 |
| 4 | 4 | 2 | $P\bar{1}$ | 1.68 | 0.67 | −0.78 | 554.52 | 0.13 | 160.75 |
| 5 | 2 | 4 | $P\bar{1}$ | 1.49 | 0.33 | −0.72 | 489.84 | 0.14 | 166.94 |
| 6 | 4 | 4 | $P2_1/c$ | 1.60 | 0.50 | −1.31 | 346.04 | 0.15 | 175.87 |
| 7 | 4 | 4 | $P2_1/c$ | 1.53 | 0.50 | −1.23 | 361.33 | 0.17 | 179.70 |
| 8 | 2 | 2 | $P\bar{1}$ | 1.62 | 0.50 | −1.21 | 340.65 | 0.18 | 166.37 |
| 9 | 4 | 4 | $P2_1/c$ | 1.64 | 0.50 | −1.15 | 338.33 | 0.19 | 175.39 |
| 10 | 4 | 4 | $P2_1/c$ | 1.57 | 0.50 | −1.15 | 353.25 | 0.19 | 170.37 |
| **nip-35DMP** | | | | | | | | | |
| 1 | 4 | 4 | $P2_1/c$ | 1.786 | 0.50 | −2.14 | 353.39 | 0.000 | 174.26 |
| 2 | 4 | 4 | $P2_1/c$ | 1.704 | 0.50 | −2.12 | 370.40 | 0.003 | 173.75 |
| 3 | 2 | 2 | $P\bar{1}$ | 1.783 | 0.50 | −2.06 | 353.99 | 0.017 | 168.28 |
| 4 | 4 | 8 | $P2_12_12_1$ | 1.573 | 0.33 | −1.24 | 514.40 | 0.042 | 176.44 |
| 5 | 4 | 2 | $P\bar{1}$ | 1.947 | 0.67 | −1.13 | 557.16 | 0.067 | 168.51 |
| 6 | 2 | 2 | $P\bar{1}$ | 1.751 | 0.50 | −1.83 | 360.46 | 0.070 | 166.19 |
| 7 | 2 | 4 | $P2_1$ | 1.541 | 0.33 | −1.08 | 525.29 | 0.079 | 167.07 |
| 8 | 2 | 4 | $P2_1$ | 1.566 | 0.33 | −1.06 | 516.59 | 0.083 | 168.82 |
| 9 | 4 | 4 | $P2_12_12_1$ | 1.758 | 0.50 | −1.77 | 359.05 | 0.084 | 167.70 |
| 10 | 4 | 2 | $P\bar{1}$ | 1.924 | 0.67 | −1.05 | 563.86 | 0.086 | 172.48 |

**3.2.1. Co-crystal of ncp with 35DMP.** In total, approximately 3000 structures were generated across all stoichiometric ratios. After eliminating duplicate structures and considering only the structures with energy within 30 kJ mol$^{-1}$ of the global minimum, 1170 structures remained, and these were then relaxed at PBE-D3 level of theory. The energy of formation of a

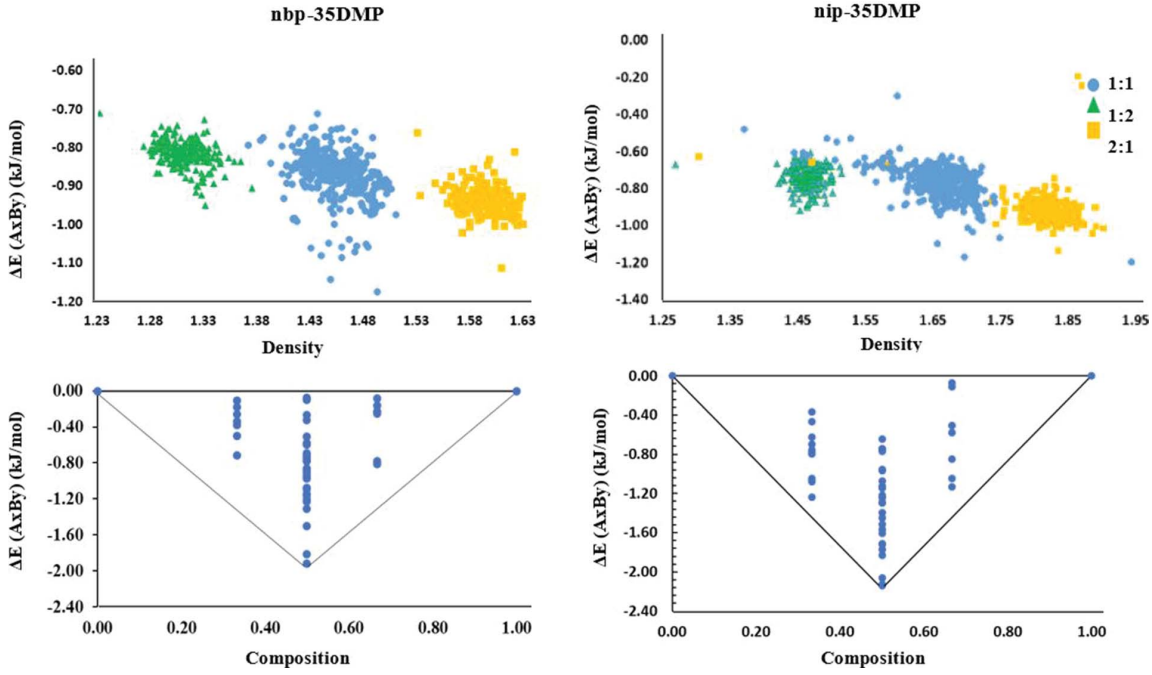


**Figure 5**
Energy landscape (top) and convex hull diagram (bottom) for the co-crystal structures of **nbp-35DMP** and **nip-35DMP**.

**Table 2**
Unit-cell parameters of VELXES (experimental structure) and of the predicted structures.

| Structure | Space group | $a$ (Å) | $b$ (Å) | $c$ (Å) | $\beta$ (°) | $V$ (Å$^3$) | $d$ (g cm$^{-3}$) |
|---|---|---|---|---|---|---|---|
| VELXES **nbp-35DMP** | $P2_1/a$ | 7.594 (11) | 25.348 (2) | 8.109 (10) | 115.867 (16) | 351.22 | 1.58 |
| Rank 1 **nbp-35DMP** | $P2_1/a$ | 7.775 | 25.046 | 8.027 | 117.70 | 334.00 | 1.66 |
| Rank 1 **nip-35DMP** | $P2_1/c$ | 8.238 | 24.064 | 7.998 | 116.931 | 353.3925 | 1.79 |

co-crystal $\Delta E$(AxBy) from pure molecular crystals was consistently positive (Table S1), which indicates the unlikelihood of co-crystal formation between **ncp** and **35DMP**, aligning with the absence of the chlorine fragment in the CSD search. (More information is available in supporting information.)

In the pure crystal structure of **ncp**, the key interactions are N—Cl···O and C—H···O. The investigation of the generated unstable co-crystal structures of **ncp-32DMP** reveals the C—H···O, N—Cl···H and C—H···N interactions (Fig. S3). Hirshfeld surfaces are mapped with shape index, and 2D fingerprint plots presented for both **ncp** and rank 1 of **ncp-35DMP** in Fig. S3.

**3.2.2. Co-crystal of nbp with 35DMP.** The generation and optimization of structures followed the previously outlined procedure. Initially, approximately 4500 structures were generated, covering various stoichiometric ratios. After filtering out high-energy and duplicate structures, 188 structures were obtained, and these were then re-optimized at PBE-D3 level of theory. The energies of formation of co-crystals $\Delta E$(AxBy) were calculated, revealing negative values for all these structures. A convex hull plot was prepared to determine the stable stoichiometric, and for metastable ones the measure of instability is dh, their height above the convex hull. Fig. 5 illustrates the energy landscape and convex hull diagram, which show that the 1:1 stoichiometry is stable. In Table S2, the generated co-crystal structures are reported. Structures were ranked based on dh (height above the convex hull).

**3.2.3. Co-crystal of nip with 35DMP.** CSP was executed as before. After removing duplicate and high-energy (>15 kJ mol$^{-1}$ from the ground state) structures, 160 structures remained and were re-optimized. Fig. 5 illustrates the energy landscape and convex hull diagram. The energies of formation of co-crystals $\Delta E$(AxBy) are negative for all these structures. Again, the 1:1 stoichiometry is on the convex hull and is thermodynamically stable. In Table S3, the generated structures are reported. Structures were ranked based on dh.

### 3.3. Intermolecular interaction patterns in structures identified by CSP

Based on the type and bond angles of the observed synthons in the CSD search analysis, the generated co-crystal structures were examined using *Mercury* software. The goal was to use these results for selecting likely co-crystal structures in CSP. In this study, each generated co-crystal structure was analyzed to identify the types of synthon interactions and its bond angles. Structures containing experimental synthons with bond angles within the observed range in CSD structures are deemed likely. As previously mentioned, the N—X···N synthon interactions are important in these compounds, the observed bond angle range being 171–180°. All low-energy crystal structures of **nbp** and **nip** exhibit N—X···N within the bond angle range 155.6–179.7°. The bond angles of N—X···N synthon interactions for the generated structures are reported in Table 1.

Notably, in both CSP co-crystals, the 1:1 ratio exhibits all the characteristics observed in CSD structures, including the presence of the N—X···N synthon interaction with bond angles within the range 171–180°, and the C—H···O synthon interaction.

Based on the analysis of CSD structures, examination of three generated **nhp-35DMP** co-crystals showed that structures lacking N—X···N halogen interactions are thermodynamically unfavorable, having either positive energy of co-crystal formation (for **ncp-35DMP**) or high dh. The interaction behavior of some lowest-energy **ncp-35DMP** co-crystals is illustrated in Fig. S3. The N—Cl···N halogen bonds were not observed in these co-crystals, just like in the CSD search.

For **nbp-35DMP** and **nip-35DMP**, only the 1:1 stoichiometry is thermodynamically stable, *i.e.* lies on the convex hull. Analysis of the generated co-crystal structures in various ratios shows that structures with ratio of 1:1 have interaction patterns similar to experimental data. In contrast, the 1:2 and 2:1 ratios do not display these patterns, which is consistent with their significant distance from the convex hull and instability.

The interaction behavior for the first ten **nbp-35DMP** and **nip-35DMP** co-crystals is also depicted in Figs. S4 and S5. The predicted convex hulls and our analysis of the interaction patterns in the generated structures align well with experimental findings, confirming that using CSD synthons and the convex hull diagram is effective for evaluating thermodynamic stability and selecting likely structures.

In the CSP of **nbp-35DMP**, the structure in rank 1 exhibits N—Br···N halogen bonding with a bond angle of 176.45° and C—H···O hydrogen bonding, mirroring the observed interaction pattern in the CSD structures [Fig. 3(*b*)]. This structure is in space group $P2_1/c$ with a 1:1 ratio, and matches VELXES [after relaxation, both structures become identical, Fig. 3(*d*)].

In the CSP of the **nip-35DMP** co-crystal, the structure ranked 1 with a ratio of 1:1 demonstrates N—I···N halogen bonding with a bond angle of 174.26° and exhibits C—H···O hydrogen bonding as anticipated, which was suggested as a likely co-crystal and its CIF file is given in the supporting information.

Table 2 presents the unit-cell parameters of VELXES and the predicted structures for **nbp-35DMP** and **nip-35DMP**. The

Hirshfeld surfaces are mapped with shape index, and 2D fingerprint plots presented for VELWIV, Predicted-**nip**, VELXES, rank 1 **nbp-35DMP** and rank 1 **nip-35DMP** in Fig. S2.

## 4. Conclusions

In conclusion, we have performed CSP of co-crystals formed by *N*-halide phthalimides (Cl, Br or I) with **35DMP**. The co-crystal structure of **nbp-35DMP** (VELXES) was known. CSP calculations revealed that **ncp** is unlikely to form co-crystals with **35DMP**. In contrast, **nbp** and **nip** are predicted to form stable co-crystals with **35DMP**. By ranking co-crystal structures based on thermodynamic stability (measured as the height above the convex hull) and considering synthons, we identified the most probable structure among the top-ranked candidates. Analysis of CSD structures highlighted the significance of N—X···N synthon interactions in similar experimental structures. The co-crystal structures ranked 1 for both **nbp-35DMP** and **nip-35DMP** exhibit N—X···N halogen bonds and C—H···O hydrogen bonds similar to those observed experimentally. The rank 1 of **nip-35DMP** is suggested as a likely co-crystal. Phonon calculations for this structure confirm its dynamical stability. Both CSD analysis and CSP calculations emphasize the central role of synthon interactions in determining crystal structures.

## Funding information

The following funding is acknowledged: Russian Science Foundation (grant No. 19-72-30043).

## References

Aakeröy, C. B. (1997). *Acta Cryst.* B**53**, 569–586.
Albright, E., Cann, J., Decken, A. & Eisler, S. (2017). *CrystEngComm*, **19**, 1024–1027.
An, K., Rhee, S., Lee, H., Kang, K.-T., Lee, C. & Kwak, J. (2020). *J. Phys. Chem. C*, **124**, 4946–4952.
Baias, M., Dumez, J.-N., Svensson, P. H., Schantz, S., Day, G. M. & Emsley, L. (2013). *J. Am. Chem. Soc.* **135**, 17501–17507.
Bennion, J. C. & Matzger, A. J. (2021). *Acc. Chem. Res.* **54**, 1699–1710.
Bolla, G., Sarma, B. & Nangia, A. K. (2022). *Chem. Rev.* **122**, 11514–11603.
Bond, A. D. & Jones, W. (2002). *Acta Cryst.* B**58**, 233–243.
Bowskill, D. H., Sugden, I. J., Konstantinopoulos, S., Adjiman, C. S. & Pantelides, C. C. (2021). *Annu. Rev. Chem. Biomol. Eng.* **12**, 593–623.
Braga, D., Grepioni, F., Maini, L. & d'Agostino, S. (2018). *Eur. J. Inorg. Chem.* **2018**, 3597–3605.
Brüning, J. & Schmidt, M. U. (2015). *J. Pharm. Pharmacol.* **67**, 773781.
Castro, M., Nicolás-Vázquez, I., Zavala, J. I., Sánchez-Viesca, F. & Berros, M. (2007). *J. Chem. Theory Comput.* **3**, 681–688.
Chakraborty, S. & Desiraju, G. R. (2018). *CrystEngComm*, **20**, 2793–2805.
Chan, E. J., Shtukenberg, A. G., Tuckerman, M. E. & Kahr, B. (2021). *Cryst. Growth Des.* **21**, 5544–5557.
Clark, T., Hennemann, M., Murray, J. S. & Politzer, P. (2007). *J. Mol. Model.* **13**, 291–296.
Day, G. M., van de Streek, J., Bonnet, A., Burley, J. C., Jones, W. & Motherwell, W. S. (2006). *Cryst. Growth Des.* **6**, 2301–2307.
Desiraju, G. R. (2007). *Angew. Chem. Int. Ed.* **46**, 8342–8356.
Dey, A., Kirchner, M. T., Vangala, V. R., Desiraju, G. R., Mondal, R. & Howard, J. A. (2005). *J. Am. Chem. Soc.* **127**, 10545–10559.
Eraković, M., Nemec, V., Lež, T., Porupski, I., Stilinović, V. & Cinčić, D. (2018). *Cryst. Growth Des.* **18**, 1182–1190.
Fotović, L., Bedeković, N. & Stilinović, V. (2021). *Cryst. Growth Des.* **21**, 6889–6901.
Frisch, M., Trucks, G., Schlegel, H., Scuseria, G., Robb, M., Cheeseman, J., Scalmani, G., Barone, V., Mennucci, B. & Petersson, G. (2013). *Gaussian 09*. Gaussian Inc., Wallingford, CT, USA.
Gale, J. D. & Rohl, A. L. (2003). *Mol. Simul.* **29**, 291–341.
Ghassemzadeh, M., Harms, K., Dehnicke, K. & Magull, J. (1994). *Z. Naturforsch. B*, **49**, 506–512.
Greenwell, C. & Beran, G. J. (2020). *Cryst. Growth Des.* **20**, 4875–4881.
Grimme, S., Antony, J., Ehrlich, S. & Krieg, H. (2010). *J. Chem. Phys.* **132**, 154104.
Groom, C. R., Bruno, I. J., Lightfoot, M. P. & Ward, S. C. (2016). *Acta Cryst.* B**72**, 171–179.
Guo, H., Puttreddy, R., Salminen, T., Lends, A., Jaudzems, K., Zeng, H. & Priimagi, A. (2022). *Nat. Commun.* **13**, 7436.
Habermehl, S., Schlesinger, C. & Schmidt, M. U. (2022). *Acta Cryst.* B**78**, 195–213.
Harper, J. K. & Grant, D. M. (2006). *Cryst. Growth Des.* **6**, 2315–2321.
Hein, R. & Beer, P. D. (2022). *Chem. Sci.* **13**, 7098–7125.
Hofmann, D. W., Kuleshova, L. N. & Antipin, M. Y. (2004). *Cryst. Growth Des.* **4**, 1395–1402.
Joubert, D. & Kresse, G. (1999). *Phys. Rev. B*, **59**, 1758–1775.
Kabova, E. A., Blundell, C. D., Muryn, C. A., Whitehead, G. F., Vitorica-Yrezabal, I. J., Ross, M. J. & Shankland, K. (2022). *CrystEngComm*, **24**, 4337–4340.
King, M. D., Blanton, T. N., Misture, S. T. & Korter, T. M. (2011). *Cryst. Growth Des.* **11**, 5733–5740.
Kresse, G. & Furthmüller, J. (1996). *Phys. Rev. B*, **54**, 11169.
Kumar, L., Leko, K., Nemec, V., Trzybiński, D., Bregović, N., Cinčić, D. & Arhangelskis, M. (2023). *Chem. Sci.* **14**, 3140–3146.
Lim, J. Y. & Beer, P. D. (2018). *Chem*, **4**, 731–783.
Lyakhov, A. O., Oganov, A. R., Stokes, H. T. & Zhu, Q. (2013). *Comput. Phys. Commun.* **184**, 1172–1182.
Macrae, C. F., Sovago, I., Cottrell, S. J., Galek, P. T. A., McCabe, P., Pidcock, E., Platings, M., Shields, G. P., Stevens, J. S., Towler, M. & Wood, P. A. (2020). *J. Appl. Cryst.* **53**, 226–235.
Mayo, S. L., Olafson, B. D. & Goddard, W. A. (1990). *J. Phys. Chem.* **94**, 8897–8909.
Momenzadeh Abardeh, Z., Salimi, A. & Oganov, A. R. (2022). *CrystEngComm*, **24**, 6066–6075.
Mukherjee, A., Tothadi, S. & Desiraju, G. R. (2014). *Acc. Chem. Res.* **47**, 2514–2524.
Mukherjee, S., Sensharma, D., Chen, K.-J. & Zaworotko, M. J. (2020). *Chem. Commun.* **56**, 10419–10441.
Oganov, A. R. (2011). *Modern Methods of Crystal Structure Prediction.* John Wiley & Sons.
Oganov, A. R. & Glass, C. W. (2006). *J. Chem. Phys.* **124**, 244704.
Oganov, A. R., Lyakhov, A. O. & Valle, M. (2011). *Acc. Chem. Res.* **44**, 227–237.
Perdew, J. P., Burke, K. & Ernzerhof, M. (1996). *Phys. Rev. Lett.* **77**, 3865–3868.
Politzer, P., Lane, P., Concha, M. C., Ma, Y. & Murray, J. S. (2007). *J. Mol. Model.* **13**, 305–311.
Politzer, P., Murray, J. S. & Clark, T. (2010). *Phys. Chem. Chem. Phys.* **12**, 7748–7757.
Politzer, P., Murray, J. S. & Clark, T. (2013). *Phys. Chem. Chem. Phys.* **15**, 11178–11189.
Raheem Thayyil, A., Juturu, T., Nayak, S. & Kamath, S. (2020). *Adv. Pharm. Bull.* **10**, 203–212.
Rappe, A. K. & Goddard, W. A. III (1991). *J. Phys. Chem.* **95**, 3358–3363.

Seidler, M., Li, N. K., Luo, X., Xuan, S., Zuckermann, R. N., Balsara, N. P., Prendergast, D. & Jiang, X. (2022). *J. Phys. Chem. B*, **126**, 4152–4159.

Singh, S. S. & Thakur, T. S. (2014). *CrystEngComm*, **16**, 4215–4230.

Stilinović, V., Horvat, G., Hrenar, T., Nemec, V. & Cinčić, D. (2017). *Chem. A Eur. J.* **23**, 5244–5257.

Sun, G., Jin, Y., Li, S., Yang, Z., Shi, B., Chang, C. & Abramov, Y. A. (2020). *J. Phys. Chem. Lett.* **11**, 8832–8838.

Teyssandier, J., Mali, K. S. & De Feyter, S. (2020). *ChemistryOpen*, **9**, 225–241.

Thakur, T. S. & Desiraju, G. R. (2008). *Cryst. Growth Des.* **8**, 4031–4044.

Tupikina, E. Y., Denisov, G. S., Antonov, A. S. & Tolstoy, P. M. (2020). *Phys. Chem. Chem. Phys.* **22**, 1994–2000.

Varadwaj, P. R., Varadwaj, A. & Marques, H. M. (2019). *Inorganics*, **7**, 40.

Wang, Y., Lv, J., Zhu, L. & Ma, Y. (2010). *Phys. Rev. B*, **82**, 094116.

Wong, S. N., Chen, Y. C. S., Xuan, B., Sun, C. C. & Chow, S. F. (2021). *CrystEngComm*, **23**, 7005–7038.

Yao, C., Guzei, I. A., Jin, Y., Ruan, S., Sun, G., Gui, Y., Wang, L. & Yu, L. (2020). *Cryst. Growth Des.* **20**, 7874–7881.